Title

Vms1p is a release factor for the ribosome-associated quality control complex

Permalink

https://escholarship.org/uc/item/0gf0v7jr

Journal

Nature Communications, 9(1)

ISSN

2041-1723

Authors

Zurita Rendón, Olga
Fredrickson, Eric K
Howard, Conor J
et al.

Publication Date

2018

DOI

10.1038/s41467-018-04564-3

Peer reviewed

Vms1p is a release factor for the ribosome-associated quality control complex

Olga Zurita Rendón[1,2], Eric K. Fredrickson[2], Conor J. Howard [3,4], Jonathan Van Vranken[2], Sarah Fogarty[1,2], Neal D. Tolley[5], Raghav Kalia[2,3,4], Beatriz A. Osuna[3,6], Peter S. Shen [2], Christopher P. Hill[2], Adam Frost [2,3,4,7] & Jared Rutter [1,2]

Eukaryotic cells employ the ribosome-associated quality control complex (RQC) to maintain homeostasis despite defects that cause ribosomes to stall. The RQC comprises the E3 ubiquitin ligase Ltn1p, the ATPase Cdc48p, Rqc1p, and Rqc2p. Upon ribosome stalling and splitting, the RQC assembles on the 60S species containing unreleased peptidyl-tRNA (60S: peptidyl–tRNA). Ltn1p and Rqc1p facilitate ubiquitination of the incomplete nascent chain, marking it for degradation. Rqc2p stabilizes Ltn1p on the 60S and recruits charged tRNAs to the 60S to catalyze elongation of the nascent protein with carboxy-terminal alanine and threonine extensions (CAT tails). By mobilizing the nascent chain, CAT tailing can expose lysine residues that are hidden in the exit tunnel, thereby supporting efficient ubiquitination. If the ubiquitin–proteasome system is overwhelmed or unavailable, CAT-tailed nascent chains can aggregate in the cytosol or within organelles like mitochondria. Here we identify Vms1p as a tRNA hydrolase that releases stalled polypeptides engaged by the RQC.

[1] Howard Hughes Medical Institute, Chevy Chase, MD 20815-6789, USA. [2] Department of Biochemistry, University of Utah School of Medicine, Salt Lake City, UT 84112, USA. [3] Department of Biochemistry and Biophysics, University of California, San Francisco, San Francisco, CA 94158, USA. [4] California Institute for Quantitative Biomedical Research, San Francisco, CA 94158, USA. [5] Molecular Medicine Program, University of Utah, Salt Lake City, UT 84112, USA. [6] Department of Microbiology and Immunology, University of California, San Francisco, San Francisco, CA 94158, USA. [7] Chan Zuckerberg Biohub, San Francisco, CA 94158, USA. These authors contributed equally: Olga Zurita Rendón, Eric K. Fredrickson, Conor J. Howard. Correspondence and requests for materials should be addressed to A.F. (email: adam.frost@ucsf.edu) or to J.R. (email: rutter@biochem.utah.edu)

Defects that impair the decoding of a messenger RNA (mRNA) can cause ribosomes to stall and distort gene expression. To prevent the accumulation of potentially toxic aberrant polypeptides, and to maintain ribosome availability, eukaryotic cells employ surveillance and clearance mechanisms, including the evolutionarily conserved ribosome-associated quality control complex (RQC). The RQC is composed of the E3 ubiquitin ligase Ltn1p, the ATPase Cdc48p and its ubiquitin-binding cofactors, and the poorly characterized proteins Rqc1p and Rqc2p—whose homologs are Listerin, VCP/p97, TCF25, and NEMF, respectively, in mammals[1–3].

Upon recognition of certain types of stalls, the 60S and 40S ribosomal subunits are split by the eRF1 homolog Dom34p, the GTPase Hbs1p, and the ATPase Rli1p[4–10]. The RQC then recognizes and assembles upon the 60S ribosomal subunit that contains an incomplete polypeptide linked to a transfer RNA (tRNA) molecule (60S:peptidyl–tRNA)[11–14]. Ltn1p ubiquitinates the nascent chain and marks it for proteasomal degradation, a process facilitated by Rqc1p through unclear mechanisms[15–17]. Rqc2p recognizes and binds to the exposed tRNA and stabilizes Ltn1p on the 60S[11,12,14]. Rqc2p also recruits charged tRNAs to the 60S subunit to catalyze elongation of the nascent protein with Carboxy-terminal Alanine and Threonine extensions (CAT tails) via a 40S-independent mechanism that is distinct from canonical translation[11,17]. This non-templated elongation of the nascent chain can mobilize potential ubiquitination sites, including lysine residues that are hidden in the ribosome exit tunnel, enhancing the efficiency of ubiquitination and the capacity of the RQC to protect cells from stochastic translation failures[17,18].

Nascent chain ubiquitination promotes extraction and proteasomal degradation of the aberrant polypeptide in a Cdc48-dependent process[2]. If the ubiquitin–proteasome system is overwhelmed or unavailable, CAT tailing enables nascent chains to form aggregates in the cytosol or within organelles like the mitochondria[19–21,22]. The critical unanswered question we investigated here concerns the identity of the hydrolase that releases ubiquitinated and CAT-tailed nascent chains from the aberrant 60S:peptidyl–tRNA for extraction and degradation by the proteasome.

Like the canonical RQC components, Vms1p is conserved throughout Eukarya and promotes protein quality control in diverse settings through its interaction with Cdc48/p97. In Saccharomyces cerevisiae, Vms1p localizes to mitochondria in response to mitochondrial stress or damage[23,24]. Mutants lacking Vms1p are sensitive to rapamycin, which impairs ribosomal protein synthesis[25,26], although the mechanism for this sensitivity is unknown. In this work, we show that Vms1p interacts genetically and physically with the RQC components, harbors an eRF1 release factor-like domain, and is required for peptidyl-tRNA hydrolysis and clearance of RQC-engaged nascent chains. This role of Vms1p in promoting proteostasis and ribosome recycling by resolving 60S:peptidyl-tRNA species expands upon the previously characterized function of Vms1p as a Cdc48/p97 binding protein and raises interesting new questions regarding the potential intersection of protein and organelle homeostasis.

Results

Vms1 physically and genetically interacts with the RQC. Because vms1Δ cells are sensitive to rapamycin, we tested whether other perturbations to translation elicit a similar phenotype. We found that the vms1Δ strain is sensitive to the protein synthesis inhibitor cycloheximide (CHX), as are other RQC mutants in a sensitizing SKI mutant background[18]. Surprisingly, deletion of any one of the RQC system components RQC1, RQC2, or LTN1,

was sufficient to reverse the lethality of the vms1Δ mutant in CHX (Fig. 1a). By contrast, deletion of the no-go decay[7,27] components DOM34 or SKI7 had no effect. These data suggest that CHX causes accumulation of an RQC product that becomes toxic in the absence of Vms1p.

The RQC assembles on a failed 60S subunit to both ubiquitinate and elongate nascent polypeptides with CAT tails. To determine whether one or both of these activities generate the putative toxic RQC product, we eliminated them separately by expressing a CAT-tailing-defective Rqc2p mutant ($RQC2^{D98Y}$)[11,14,21] or a variant of Ltn1p deficient in ubiquitination ($LTN1^{W1542E}$)[17,28]. CAT tailing by Rqc2p was dispensable, while ubiquitination by Ltn1p was essential for conferring CHX sensitivity on a vms1Δ mutant strain—indicating that the toxic species in this context depends on ubiquitination rather than CAT-tailing (Fig. 1b). Presumably because of its proposed role in nascent chain ubiquitination[17], and similar to RQC2 and LTN1 (Fig. 1b), plasmid expression of wild-type (WT) RQC1 was sufficient to reverse the rescue of vms1Δ cycloheximide sensitivity conferred by RQC1 deletion (Supplementary Fig. 1a).

In light of the association between Vms1 activity and mitochondrial stress, we examined the ability of these single and double mutant strains to grow in glycerol medium, which requires mitochondrial respiration. Interestingly, deletion of LTN1—but not RQC1, RQC2, or DOM34—strongly impaired glycerol growth of vms1Δ cells (Supplementary Fig. 1b). Similarly, ski7Δ vms1Δ double mutant cells also exhibited partially impaired glycerol growth (Supplementary Fig. 1b). These data indicate a specific relationship between Vms1p, RQC function, and mitochondrial homeostasis, which is consistent with a recent report that stalled polypeptides that cannot be ubiquitinated by Ltn1p accumulate within and compromise mitochondria—underscoring the reversal of the genetic interaction we observed between LTN1 and VMS1 on glucose vs. glycerol[22].

These genetic interactions prompted us to determine whether Vms1p physically interacts with members of the RQC, as has been reported previously[1,3,22]. As expected, isolation of Rqc2p-HA co-immunoprecipitated Vms1p-V5. In contrast, Rqc1p-HA or Ltn1p-HA showed minimal Vms1p interaction (Fig. 1c and Supplementary Fig. 1c-d). Consistently, both Rqc2p and Vms1p co-migrated with the 60S ribosome subunit during sucrose gradient sedimentation following CHX treatment (Fig. 1d, Supplementary Fig. 1e). Co-migration of Vms1p with the 60S ribosome was not affected by either deletion of RQC2 or by expression of WT or a CAT-tailing defective, D98Y, mutant of Rqc2p (Supplementary Fig. 1e). Similarly, neither deletion nor overexpression of Vms1p from the strong GAL1 promoter in galactose medium had any effect on the co-migration of Rqc2p with the 60S ribosomal subunit (Supplementary Fig. 1e, f).

Vms1p is required for resolving RQC substrates. The genetic and physical interactions described above motivated us to evaluate whether RQC substrates accumulate in VMS1 mutant cells. We utilized a well-characterized mRNA that encodes FLAG-tagged green fluorescent protein (GFP) followed by a hammerhead ribozyme that self-cleaves in vivo (FLAG-GFP^{Rz}, Fig. 2a)[6,11] to generate a truncated mRNA encoding FLAG-GFP without a stop codon or poly-A tail. Translation of this mRNA triggers ribosome stalling and targeting to the RQC. Deletion of SKI7 enhances expression of GFP by inhibiting degradation of the cleaved mRNA[29]. We confirmed that deletion of RQC1, RQC2, and LTN1 each lead to accumulation of FLAG-GFP^{Rz}, whereas the nascent chain failed to accumulate in the ski7Δ single mutant (Fig. 2a–c, Supplementary Fig. 2a). Loss of Vms1p also led to accumulation of FLAG-GFP^{Rz} to a level similar to that observed
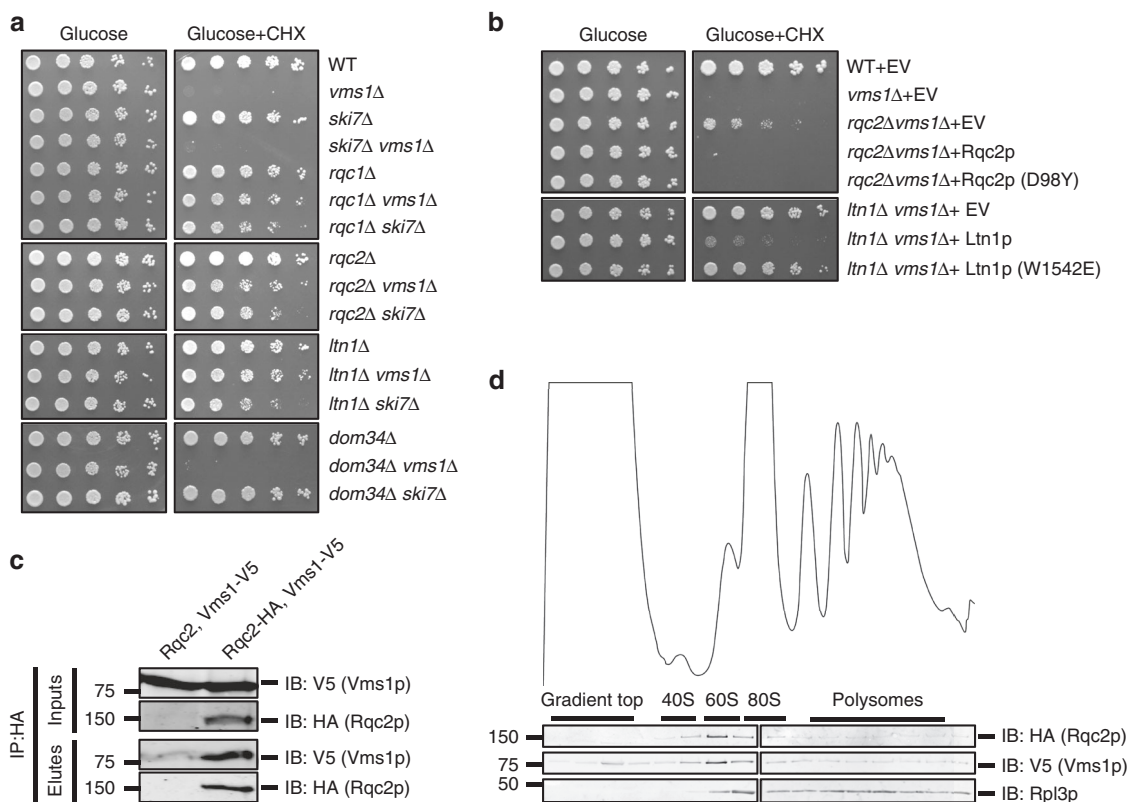
Fig. 1 Vms1 physically and genetically interacts with the RQC. **a, b** Serial dilutions of indicated strains were spotted on media containing glucose or glucose supplemented with cycloheximide (CHX). EV empty vector. **c** Immunoprecipitation using anti-HA antibody in the strains *rqc2Δ vms1Δ* expressing Rqc2p and Vms1p-V5 (control) or Rqc2p-HA and Vms1p-V5. Immunoblotting of HA and V5 were used to identify Rqc2p and Vms1p, respectively. **d** Polysome profile of the *rqc2Δ vms1Δ* strain expressing Rqc2p-HA and Vms1p-V5 treated with CHX prior to fractionation using sucrose density centrifugation. The sedimentation of ribosomal particles was inferred from the A_{254} profile (40S, 60S, 80S, and polysomes) and the distribution of the 60S subunit was confirmed by immunoblotting of the ribosomal subunit, Rpl3p. Immunoblotting of HA and V5 was used to detect Rqc2p and Vms1p, respectively

for the core RQC components (Fig. 2a–c, Supplementary Fig. 2b). Combination of *VMS1* deletion with the deletion of *RQC1*, *RQC2*, and *LTN1* had no additive effect on GFP accumulation (Fig. 2b). Immunoblot analysis showed similar results for the single, double, and triple mutant strains, in which RQC2-dependent, high-molecular-weight aggregates are also apparent (Fig. 2c, Supplementary Fig. 2b)[19–21]. Loss of *DOM34* led to decreased accumulation of GFP fluorescence, even in the *vms1Δ* strain, consistent with the upstream role of Dom34p in ribosome splitting and suggestive of alternative pathways for degrading nascent chains when the Dom34p/Hbs1p subunit splitting activity is unavailable (Fig. 2a–c). Interestingly, accumulation of FLAG-GFP[Rz] in *vms1Δ* mutant cells occurs despite lower mRNA abundance (Supplementary Fig. 2c).

In addition to the FLAG-GFP[Rz] construct, which generates a cytosolic RQC substrate, we also examined RQC activity on fumarase, which is encoded by the *FUM1* gene and co-translationally imported into the mitochondria[30]. As with FLAG-GFP[Rz], fluorescence from the Fum1-FLAG-GFP[Rz] construct, expressed from the native *FUM1* promoter, was also maintained at a low level in the *ski7Δ* mutant strain (Fig. 2d). Deletion of *VMS1*, *RQC1*, *RQC2*, or *LTN1* each led to profound accumulation of GFP fluorescence, almost all of which colocalized with mitochondria-targeted red fluorescence protein (mtRFP). The *vms1Δ*, *rqc1Δ*, and *ltn1Δ* mutants, which retain Rqc2p and CAT-tailing activity, all exhibited Fum1-GFP aggregates within or near mitochondria, comparable to recent observations of other mitochondria-destined nascent chains[28] (Fig. 2d). The *rqc2Δ* mutant exhibited a more uniformly mitochondrial localization

pattern (Fig. 2d), consistent with the model that CAT tailing mediates intra-mitochondrial aggregation of polypeptides that stall during co-translational import[28]. Together, these data demonstrate that Vms1p is required for the degradation of substrates derived from truncated mRNAs, whether they are destined for a membranous organelle or the cytosol.

Vms1p is structurally homologous to tRNA hydrolases. Understanding of how Vms1p facilitates the clearance of stalled translation products was guided by our recent crystal structure determination of a portion of *S. cerevisiae* Vms1p (Fig. 3a, b)[31]. This structure includes the highly conserved central region of Vms1p, which we named the mitochondrial targeting domain (MTD) because it is necessary and sufficient for mitochondrial localization[23]. This localization activity requires a hydrophobic groove along the region of the MTD where the LRS interacts and direct binding to ergosterol peroxide[31]. Intriguingly, the Vms1p MTD structure resembles structures of the catalytic domain of eukaryotic peptide chain release factor subunit 1 (eRF1), as well as Dom34p and RNaseE, which both resemble tRNA hydrolases[32–35] (Fig. 3b, Supplementary Fig. 3a). The only region of the Vms1p MTD that diverges substantially from the release factor fold is the face of the MTD that mediates ergosterol peroxide binding and mitochondrial localization[31] (Fig. 3b).

Sequence alignment showed that although Vms1p lacks a strict GGQ motif characteristic of eRF1p, it does possess an invariant glutamine that can align with the catalytic glutamine of eRF1 (Fig. 3c). In yeast Vms1p, this glutamine residue is
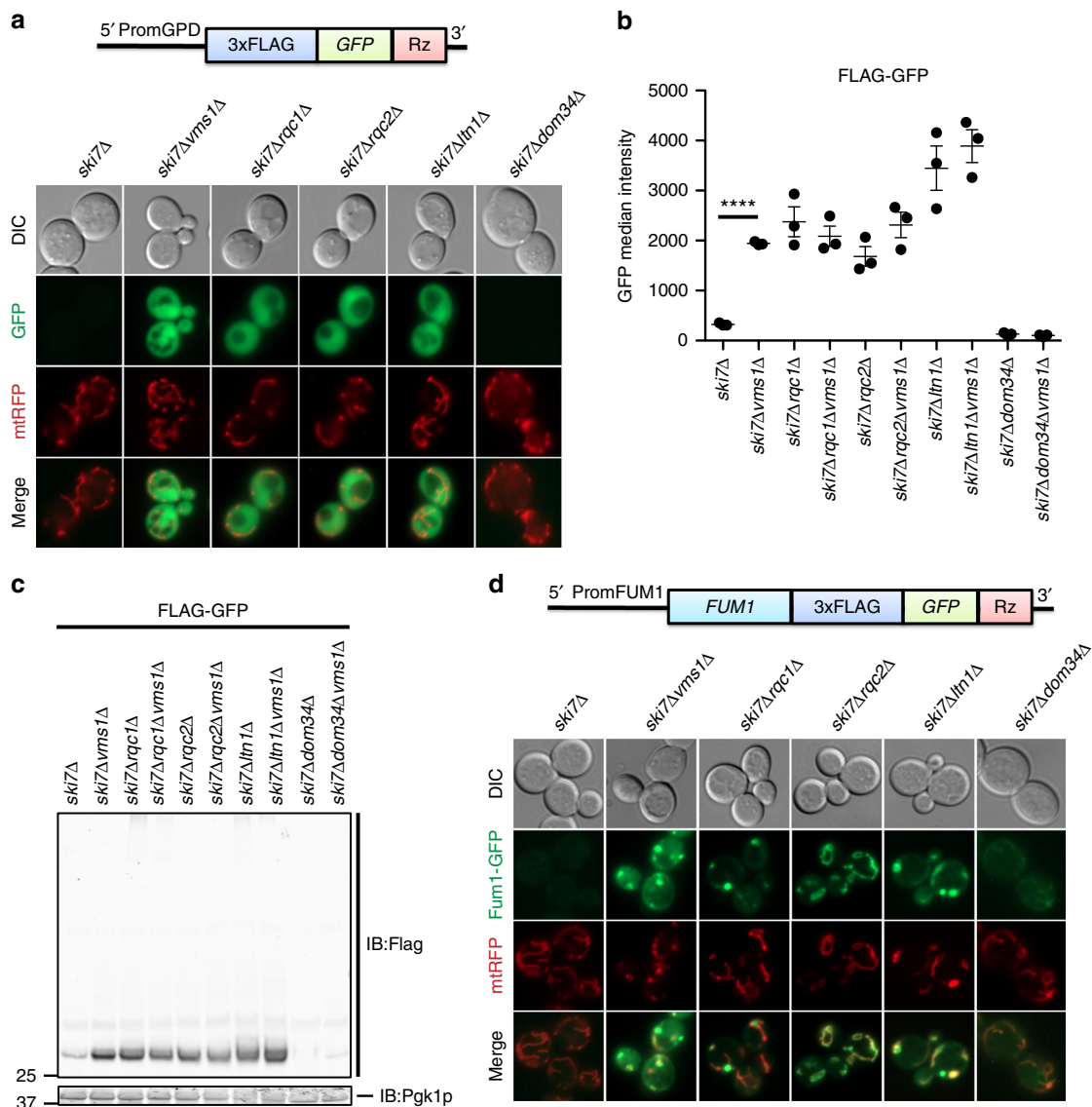
Fig. 2 Vms1p is required for resolving RQC substrates. **a** Fluorescence microscopy analysis of the indicated strains expressing the FLAG-GFP[Rz] construct under the GPD promoter and the mitochondrial marker, mtRFP. **b** Flow cytometry quantifications of FLAG-GFP accumulation in the indicated strains. Median GFP intensity values are plotted ($n = 3$, mean ± s.e.m. [****]$P < 0.0001$, The p value was calculated using unpaired Student's t-test). **c** Immunoblot analysis of indicated strains expressing the FLAG-GFP[Rz] construct. Immunoblotting of Flag was used to detect the accumulation of the stalled construct. Pgk1p was used as loading control. **d** Fluorescence microscopy analysis of the indicated strains expressing the Fum1-FLAG-GFP[Rz] construct expressed from the *FUM1* endogenous promoter and the mitochondrial marker, mtRFP

embedded within a GGSQ motif that is reminiscent of the eRF1 catalytic GGQ, while in other species the conservation other than the initial glycine and glutamine is less apparent (Fig. 3c, d). The Vms1p MTD lacks similarity to the non-catalytic eRF1 domain 1, which discriminates stop codons from sense codons[35]. This is consistent with Vms1p functioning in stop codon-independent tRNA hydrolysis within a 60S, rather than 80S, ribosome.

These observations inspired us to determine whether Vms1p enables the extraction of failed translation products from the stalled 60S by hydrolyzing the ester bond anchoring them to tRNA. We asked which residues and regions are required for the genetic functions of *VMS1*. We first tested an HbφT motif just N terminal to the conserved 'GxxQ' motif that mediates ribosome interactions of eRF1 (Fig. 3c, d). Vms1p mutants of these residues, H279A, H283A, R284A, and T286A, were indistinguishable from WT, while the Y285A mutant exhibited a partial CHX

sensitivity (Fig. 3f). In contrast, mutation of the 'GxxQ' residues G292 and Q295 and the highly conserved R288 residue conferred strong loss-of-function phenotypes (Fig. 3e). Deletion of S294 to convert the GGSQ of *S. cerevisiae* Vms1p into a GGQ motif, as in eRF1, also abrogated *VMS1* function (Fig. 3e). While all of these 'GxxQ 'mutants failed to confer resistance to 200 ng ml^{-1} CHX, only the R288A and G292A/G293A mutants were inactive at the lowest (100 ng ml^{-1}) concentration of CHX tested (Fig. 3e). Interestingly, both of these mutants also failed to rescue glycerol growth in an *ltn1Δ vms1Δ* double mutant, whereas wild-type *VMS1* and the other mutants did rescue growth (Supplementary Fig. 3b). The R288A, G292A/G293A, and Q295L mutants also exhibited enhanced accumulation of FLAG-GFP[Rz] in the *ski7Δ* background similar to the *vms1Δ* mutant (Supplementary Fig. 3d). Importantly, the Vms1p mutants interact normally, if not more strongly, with Rqc2p based on co-immunoprecipitation experiments (Supplementary Fig. 3e). In light of these observations, we
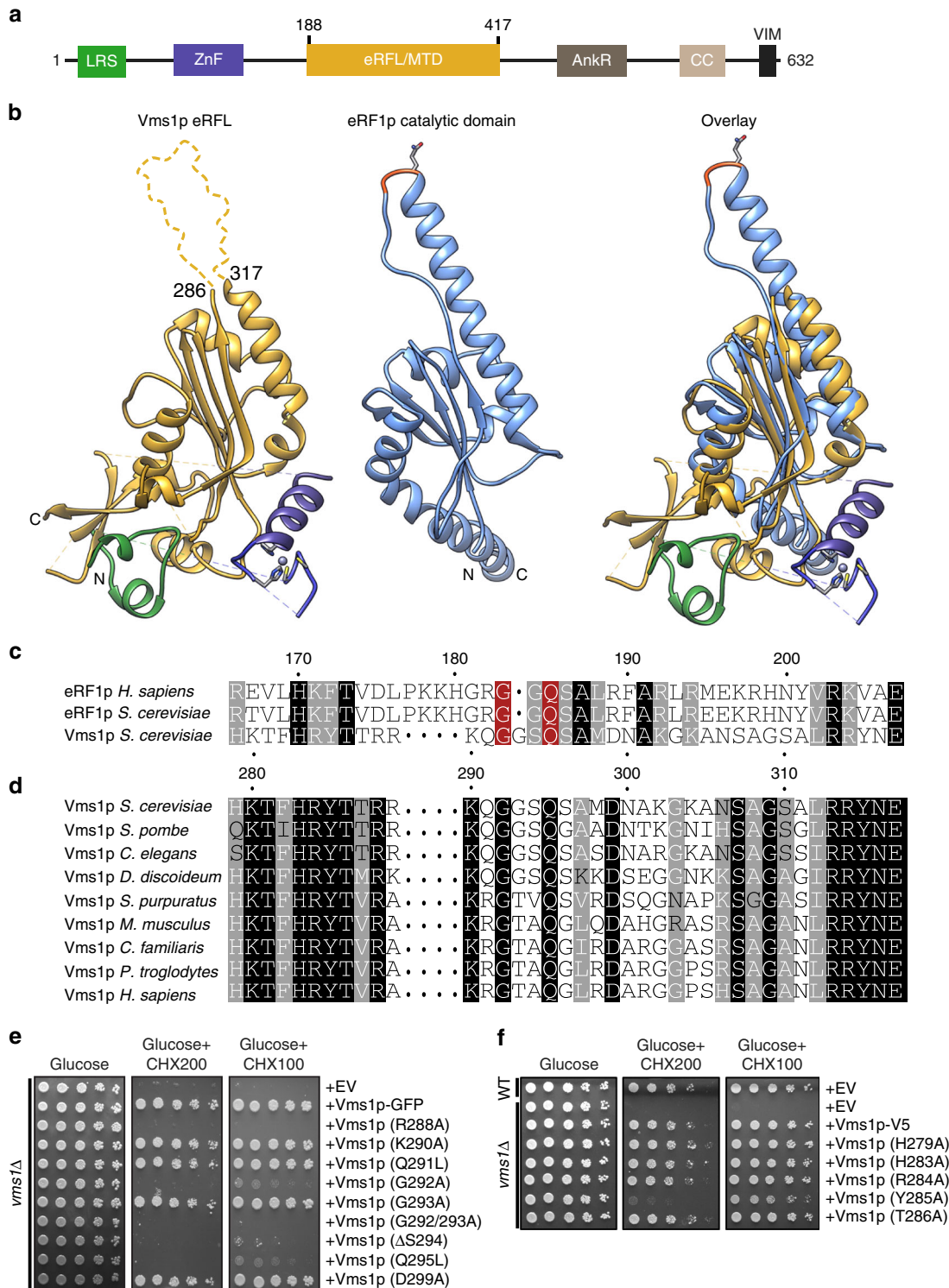
Fig. 3 Vms1p is structurally homologous to tRNA hydrolases. **a** Domain structure of Vms1p. LRS leucine-rich sequence, ZnF zinc finger, MTD/eRFL mitochondrial targeting domain/eRF1-like, AnkR ankryin repeat, CC coil–coil, VIM VCP-interacting motif. Residues 188–417 represent the MTD/eRFL boundaries. **b** Structural alignment of Vms1p (left, 5WHG[31]) and eRF1p (middle, 3JAHii[35], residues 144–280). Dashed lines indicate connections made by residues that are not resolved in the Vms1p crystal structure. The GGQ (red) loop of eRF1p is ordered in the ribosome-bound structure shown here. **c** Sequence alignment of Vms1p and eRF1p. White letters with gray, black, or red background indicates similarity, identity, or GxxQ residues, respectively. **d** Sequence alignment of Vms1p orthologs across the GxxQ region. Coloring as in **c**. **e**, **f** Serial dilutions of indicated strains were spotted on media containing glucose or glucose supplemented with cycloheximide (CHX). EV empty vector

hereafter refer to the MTD as the MTD/eRFL domain, where eRFL refers to eRF1-like.

In addition to these loop residues, the ability of Vms1p to confer complete CHX resistance in both $vms1\Delta$ and $ski7\Delta\ vms1\Delta$ also required the p97/valosin-containing protein (VCP)-interacting motif (VIM), which mediates interaction with Cdc48p/VCP/p97[22] (Supplementary Fig. 3c). Interestingly, the VIM is not required for growth of the $ltn1\Delta\ vms1\Delta$ double mutant on glycerol (Supplementary Fig. 3c), which indicates that mitochondrial homeostasis can be maintained even without Cdc48p binding.

Vms1p exhibits tRNA hydrolase activity towards RQC substrates. To directly test whether Vms1p catalyzes peptidyl-tRNA hydrolysis, we utilized our recently described *S. cerevisiae* in vitro translation (ScIVT) system to monitor the synthesis and fate of a robust stalling reporter and its peptidyl-tRNA intermediate[17]. RQC-intact extracts translate this reporter, split the stalled 80S ribosome into constituent 60S and 40S subunits, elongate the nascent chain with a CAT tail, and ubiquitinate exposed lysine residues. These extracts also hydrolyze the peptidyl-tRNA ester bond to generate the released polypeptide[17] (Fig. 4a). We observed that extracts prepared from $vms1\Delta$ mutant cells also produced peptidyl-tRNA conjugates, but loss of the peptidyl-tRNA species and appearance of the released translation product were slower than in WT extracts (Fig. 4a, b). This is somewhat obscured by the fact that the $vms1\Delta$ mutant has lower overall translation, which leads to a decreased amount of the free nascent

chain and peptidyl-tRNA conjugates. We performed a similar experiment in the $ski7\Delta$ and $ski7\Delta\ vms1\Delta$ mutant strains and found that in the $ski7\Delta$ background the deletion of *VMS1* conferred a much more obvious stabilization of the peptidyl-tRNA species and qualitatively delayed release of the polypeptides (Fig. 4c, d). In this $ski7\Delta$ background, deletion of *RQC2* conferred a modest stabilization of the peptidyl-tRNA conjugate and had little effect on the $vms1\Delta$ mutant (Supplementary Fig. 4a). We next purified full-length and C-terminally truncated (1–417) *S. cerevisiae* Vms1p and found that each of these proteins dramatically accelerated the production of the released polypeptide in a dose-dependent manner in WT, $rqc2\Delta$ and $vms1\Delta$ extracts (Fig. 4e, Supplementary Fig. 4b). Importantly, the 1–417 truncation mutant lacks the C-terminal VIM domain and is unable to interact with Cdc48p (Supplementary Fig. 3e). We therefore conclude that while the Vms1p–Cdc48p interaction is important for CHX resistance and other RQC-related functions that are relevant to the *VMS1* genetic interactions, Vms1p association with Cdc48p is dispensable for peptidyl-tRNA hydrolysis.

We next tested release factor activity of the MTD/eRFL domain structure-based mutants described above. The Q295L, G292A, and ΔS294 mutants also exhibited strongly impaired release factor activity (Fig. 4f and Supplementary Fig. 4c). Consistent with the stronger growth phenotypes we observed on different concentrations of CHX and on glycerol, R288A and G292A/G293A mutants had no hydrolysis activity, even at 10-fold higher concentration than the concentration at which WT Vms1p catalyzed complete tRNA release (Fig. 4f).
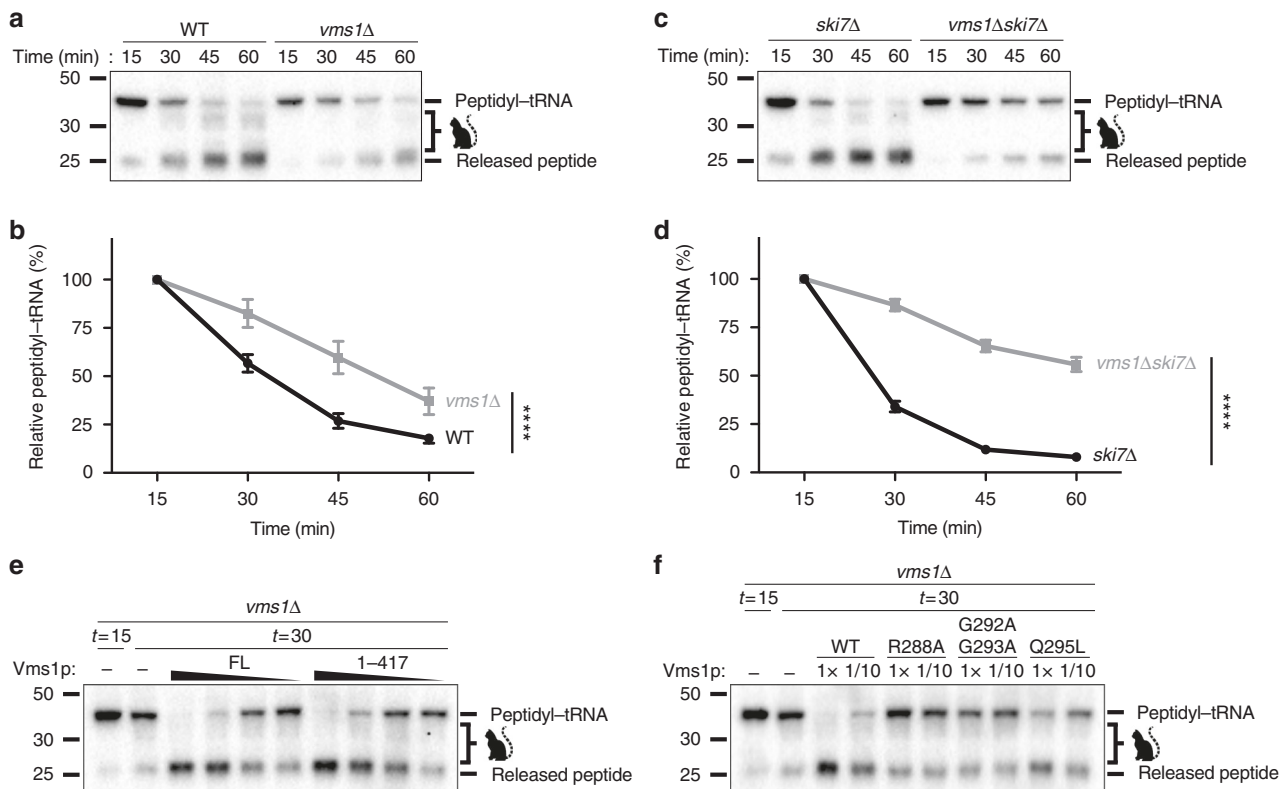

Fig. 4 Vms1p exhibits tRNA hydrolase activity towards RQC substrates. **a** Time courses of *S. cerevisiae* in vitro translation (ScIVT) reactions prepared with a truncated mRNA (lacking a stop codon). Extract genotypes are indicated above. Peptides that have been CAT-tailed and released are denoted with a cat tail icon. **b** Quantification of peptidyl-tRNA species in **a**. Mean ± s.e.m.; n = 6. ****$P < 0.0001$. The p value was calculated using a two-way ANOVA. **c** Time courses of ScIVT reactions prepared as in **a**. **d** Quantification of peptidyl-tRNA species in **c**. Mean ± s.e.m., n = 8. ****$P < 0.0001$. The p value was calculated using a two-way ANOVA. **e** ScIVT reactions prepared as in **a** with a $vms1\Delta$ extract. At $t = 15$, buffer (−) or pure protein was added. Slopes indicate a titration series of decreasing protein concentrations (see Methods). FL full length Vms1, 1–417 N terminus through eRFL domain. **f** ScIVT reactions prepared as in **a** with a $vms1\Delta$ extract. At $t = 15$, buffer, WT (1–417) protein, or mutant (1–417) protein was added

Discussion

Our data have identified a key constituent of the RQC pathway in Eukarya: a tRNA hydrolase that liberates failed polypeptides from the aberrant 60S:peptidyl-tRNA species that accumulate when ribosomes stall. Without this activity, translation products remain anchored in 60S ribosomes, which therefore cannot be recycled for future use. The dual functions of the Vms1p MTD/eRFL identified here as an RQC release factor and previously as a targeting domain in mitochondrial stress responses portend exciting future work at the intersection of proteostasis and organelle homeostasis. We have previously reported that Vms1p localizes to mitochondria under conditions of mitochondrial damage or cellular stressors, including rapamycin treatment, by binding to the oxidized sterol ergosterol peroxide[22,23,31]. The MTD/eRFL domain is necessary and sufficient for this localization, which is mediated by a direct interaction between a face of the MTD/eRFL domain that should remain exposed even when the domain is in the 'A-site' of the 60S and the catalytic GGSQ loop is presumably reaching into the peptidyl transferase center to catalyze hydrolysis of the peptidyl-tRNA ester bond. While the relationship between mitochondrial localization and RQC-coupled release factor activity remains unclear, it is intriguing to speculate that this is indicative of a role for Vms1p—and the RQC as a whole—in the response to mitochondrial stress. Consistent with this possibility, $ltn1\Delta$ $vms1\Delta$ and $ski7\Delta$ $vms1\Delta$ double mutant cells exhibit impaired glycerol growth, which correlates with impaired mitochondrial respiration[28].

The diseases associated with even subtle distortions in protein quality control underscore the importance of the activity of Vms1p as a release factor for the RQC. Among many other examples, hypomorphic mutations in the RQC-associated ubiquitin E3 ligase, Listerin (Ltn1p in yeast), lead to profound neurodegeneration in mice[36]. As we show, Vms1p protects cells from inadequate Ltn1p activity by releasing CAT tailed nascent chains from stalled 60S ribosomes. In so doing, Vms1p rescues these ribosome subunits for future use and defends proteostasis from translation products whose accumulation could otherwise cause disease. We therefore propose that Vms1p is required for the resolution of peptidyl-tRNA conjugates of stalled nascent chains in the cytosol as well as those destined for organelles like the mitochondria, where it might mediate a particular role in protecting mitochondria from proteostasis challenges.

Methods

Yeast strains and growth conditions. *S. cerevisiae* BY4741 (*MATa, his3 leu2 met15 ura3*) was used as the wild-type strain. Each mutant was generated in diploid cells using a standard PCR-based homologous recombination method. The genotypes of all strains used in this study are listed in Supplementary Table 1. Yeast transformations were performed by the standard TE/LiAc method and transformed cells were recovered and grown in synthetic complete glucose medium lacking the appropriate amino acid(s) for selection. The medium used included YPA and synthetic minimal medium supplemented with 2% glucose or 3% glycerol. Cycloheximide was added at a final concentration of 100 ng ml^{-1} or 200 ng ml^{-1} when indicated.

All plasmid constructs were generated by PCR and cloned into the yeast expression vectors pRS413, pRS14 or pRS416 as indicated in Supplementary Table 2.

Growth assays were performed using synthetic minimal media supplemented with the appropriate amino acids and indicated carbon source. For plate-based growth assays, overnight cultures were back-diluted to equivalent optical densities (ODs) and spotted as 10-fold serial dilutions. Cells were grown at 30 °C.

Immunoprecipitations. p^{VMS1}-VMS1-V5 (or VMS1 mutant) was co-expressed with an endogenous promoter-His$_6$-HA$_2$ tagged RQC component (RQC1, RQC2, LTN1) in the cognate double mutant strain. Approximately 50 ODs were harvested in log phase and resuspended in IP buffer (20 mM Tris pH 7.4, 50 mM NaCl, 0.2% Triton X-100), vortexed 10 × 1 min, clarified via centrifugation, and added to anti-HA magnetic beads (Thermo Scientific #88836). After 4 h of incubation, beads were pelleted via magnet and washed 4× with 1 ml of IP buffer. Proteins were eluted with 50 µl of 2× Laemmli buffer (20% glycerol, 125 mM Tris-HCl pH 6.8, 4%

sodium dodecyl sulfate (SDS), 0.02% bromophenol blue). Source data can be found in Supplementary Fig. 5a.

Polysome profiling. Yeast cultures were grown to OD$_{600}$ ~1, cycloheximide was added to a final concentration of 0.05 mg ml^{-1}, and cells were harvested by centrifugation 5 min later. Cell pellets were washed in buffer A (20 mM Tris-HCl pH 7.4, 50 mM KCl, 10 mM MgCl$_2$, 1 mM dithiothreitol (DTT), 100 µg ml^{-1} cycloheximide, 1 × RNAsecure (Ambion), and 1× yeast protease inhibitor (Sigma)). Pellets were weighed and resuspended in 1.3 volumes of Buffer A. An equal volume of glass beads was added and suspensions were vortexed for 30 s for a total of 8 times interspersed with 1 min of incubation on ice. Following centrifugation at 3000 × g for 5 min, supernatant was centrifuged at 11,300 × g for 2 min at 4 °C, after which supernatant was centrifuged at 11,300 × g for 10 min. Protein extracts were overlaid onto a linear sucrose gradient of 15–50% and centrifuged at 234,600 × g for 90 min. The gradients were passed through a continuous-flow chamber and monitored at 254 nm with an ultraviolet absorbance detector (ISCO UA-6) to obtain ribosomal profiles. Fractions (16) were collected, resuspended in 2× Laemmli sample buffer supplemented with 2.5% beta-mercaptoethanol, and analyzed by western blotting. Source data can be found in Supplementary Fig. 5b.

SDS-PAGE. Whole-cell extracts were prepared from 3 to 5 ODs of cells at OD$_{600}$~1.5 by solubilization in 250 µl of 2 M LiAc, incubated for 8 min on ice followed by centrifugation at 0.9 × g for 5 min at 4 °C. The pellet was resuspended in 250 µl of 0.4 M NaOH and incubated on ice for 8 min followed by centrifugation at 16,000 × g for 3 min. Next, the pellet was resuspended in 1× Laemmli buffer with 2.5% beta-mercaptoethanol, boiled for 5 min, and centrifuged at 0.9 × g for 1 min. Supernatants were collected and loaded onto acrylamide/bisacrylamide (37.5:1) gels. Subsequent immunoblotting was done with the indicated antibodies: HA (PRB-101C-200), V5 (ab9116), FLAG (F7425), Pgk1: (ab113687), and Rpl3 (scRPL3). Source data can be found in Supplementary Fig. 6.

Fluorescence microscopy. WT (BY4741) or derived mutant strains were transformed with a plasmid expressing mitochondria-targeted (ATPase subunit, Su9) RFP, mtRFP, and plasmids expressing Flag$_3$His$_6$-GFP-Rz or FUM1-Flag$_3$His$_6$-GFP-Rz under the *GPD* or native *FUM1* promoter, respectively. The cells were grown to mid-log phase and imaged using the Axio Observer Z1 imaging system (Carl Zeiss). Digital fluorescence and differential interference contrast images were acquired using a monochrome digital camera (AxioCam MRm) and analyzed using the Zen 2 software (Carl Zeiss).

Fluorescence-assisted cell sorting. GFP-expressing strains and untransformed control were grown to OD$_{600}$ ~1 and pelleted by centrifugation at 100 × g for 5 min. Cell pellets were washed once in 1× phosphate-buffered saline (PBS) buffer, resuspended in 1 ml of 1× PBS, and analyzed using the BDFACSCanto Analyzer (488 laser and optical filter FITC). A total of 30,000 events were measured and the median values of three independent biological replicates were analyzed by one-way analysis of variance (ANOVA; Bonferroni correction analysis) with a confidence interval of <0.05 using the statistics software: Graphpad Prism 6. Additionally, $ski7\Delta$, $ski7\Delta vms1\Delta$, and strains in Supplementary Fig. 3 were compared via unpaired Student's *t*-test (two-tailed) confidence interval value set to $p < 0.05$. Error bars represent standard error of the mean.

Protein expression and purification. For the His$_{12}$ tagged proteins, constructs were transformed into JRY1734 (pep4::HIS3 prb1::LEU2 bar1::HISG lys2::GAL1/10-GAL4) and grown in synthetic media lacking Uracil with 3% glycerol and 2% ethanol. When the OD$_{600}$ reached ~0.5, 0.5% galactose was added to the cultures, which were grown for another 6 h before harvesting by centrifugation, washing of the pellet with sterile H2O, and flash freezing in liquid nitrogen. Cells were lysed using a pulverizer (SPEX SamplePrep 6870), and the lysed powder was thoroughly resuspended in lysis buffer (20 mM Tris pH 8.0, 300 mM NaCl, 5% glycerol) supplemented with protease inhibitors (aprotinin, leupeptin, pepstatin A, and PMSF) (Sigma). The resuspended lysate was clarified by centrifugation and added to Ni-NTA resin (Qiagen #30250) for 1 hour, washed with 10 CV of lysis buffer, 10 CV of lysis buffer with 40 mM imidazole, and eluted with lysis buffer made up with 250 mM imidazole. Eluted protein was dialyzed into IVT-compatible buffer (20 mM HEPES-KOH pH 7.4, 150 mM KOAc, 5% glycerol, 2 mM DTT) and concentrated.

S. cerevisiae in vitro translation. Preparation of in vitro translation extracts, mRNA, and in vitro translation reactions was performed as previously described [17]. Briefly, *S. cerevisiae* strains were cryo-lysed and cell debris was cleared by sequential centrifugation before dialysis into fresh lysis buffer. mRNAs were generated by run-off transcription from PCR-amplified templates of 3xHA-NanoLuciferase to produce transcripts lacking a stop codon and 3′-untranslated region (truncated quality control substrate). Transcription products were capped and extracted prior to freezing for use in ScIVTs. For ScIVT reactions, extracts were first treated with MNase to remove endogenous mRNAs and then

supplemented with 480 ng mRNA to initiate translation. Reaction aliquots were sampled at indicated time points by quenching in 2× Laemmli Sample Buffer. Proteins were separated by SDS-PAGE, and hemagglutinin (HA)-tagged translation products were visualized by immunoblotting (Roche 3F10). To quantify release, the abundance of peptidyl-tRNA was measured with Fiji (https://imagej. net/Fiji) and normalized as percentage of the initial 15 min time point. Mean values of at least 6 technical replicates were analyzed and plotted in Prism (GraphPad software). P-values were calculated using a two-way ANOVA. Error bars represent standard error of the mean. The ramps of Fig. 4e represent a decreasing titration series of 4.2 μM, 0.42 μM, 0.21 μM, and 0.105 μM final protein concentrations. In Fig. 4f and Supplementary Fig. 4c, 1× and 1/10 refer to final protein concentrations of 4.2 μM and 0.42 μM, respectively. Source data can be found in Supplementary Fig. 7.

Quantitative RT-PCR. RNA was purified from 40 ml of yeast cultures grown to OD_{600} ~1. Pelleted cells were washed once with water and resuspended in 700 μl of Trizol reagent (Ambion). An equal volume of glass beads was added and suspensions were vortexed for 30 s intervened with 1 min rest intervals. Next, the manufacture's protocol from the Direct-zol kit (Zymo research: R2050-11-330) was followed. Complementary DNA (cDNA) was obtained from 0.5 μg of purified RNA using the High-capacity cDNA Reverse Transcription kit (4368814) from Applied Biosystems. Quantitative PCR was performed using the LightCycler 480 SYBR Green I Master (04707516001) from Roche and using a FLAG-HIS and Actin primer pairs. Quantitative PCR analysis was done by Absolute Quantification/2nd derivative of three independent biological replicates, each performed in triplicate. The statistical analysis of mRNA transcript abundance was done after normalization with Actin. The statistics software Graphpad Prism 6 was used to perform Student's t-test (unpaired two-tail) with a confidence interval value of $p < 0.05$. Error bars represent standard error of the mean.

Data availability. The authors declare that the data supporting the findings of this study are available within the paper and its supplementary information files. Further relevant data on the genes studied in this manuscript (VMS1: YDR049W, RQC1: YDR333C, RQC2: YPL009C, LTN1: YMR2476, SKI7: YOR076C, DOM34: YNL01W) can be found at: https://www.yeastgenome.org.

References

1. Brandman, O. et al. A ribosome-bound quality control complex triggers degradation of nascent peptides and signals translation stress. *Cell* **151**, 1042–1054 (2012).
2. Verma, R., Oania, R. S., Kolawa, N. J. & Deshaies, R. J. Cdc48/p97 promotes degradation of aberrant nascent polypeptides bound to the ribosome. *eLife* **2**, e00308 (2013).
3. Defenouillere, Q. et al. Cdc48-associated complex bound to 60S particles is required for the clearance of aberrant translation products. *Proc. Natl. Acad. Sci. USA* **110**, 5046–5051 (2013).
4. van den Elzen, A. M. et al. Dissection of Dom34-Hbs1 reveals independent functions in two RNA quality control pathways. *Nat. Struct. Mol. Biol.* **17**, 1446–1452 (2010).
5. van den Elzen, A. M., Schuller, A., Green, R. & Seraphin, B. Dom34-Hbs1 mediated dissociation of inactive 80S ribosomes promotes restart of translation after stress. *EMBO J.* **33**, 265–276 (2014).
6. Kobayashi, K. et al. Structural basis for mRNA surveillance by archaeal Pelota and GTP-bound EF1alpha complex. *Proc. Natl. Acad. Sci. USA* **107**, 17575–17579 (2010).
7. Tsuboi, T. et al. Dom34:hbs1 plays a general role in quality-control systems by dissociation of a stalled ribosome at the 3' end of aberrant mRNA. *Mol. Cell* **46**, 518–529 (2012).
8. Shoemaker, C. J., Eyler, D. E. & Green, R. Dom34:Hbs1 promotes subunit dissociation and peptidyl-tRNA drop-off to initiate no-go decay. *Science* **330**, 369–372 (2010).
9. Shoemaker, C. J. & Green, R. Kinetic analysis reveals the ordered coupling of translation termination and ribosome recycling in yeast. *Proc. Natl. Acad. Sci. USA* **108**, E1392–E1398 (2011).
10. Chen, L. et al. Structure of the Dom34-Hbs1 complex and implications for no-go decay. *Nat. Struct. Mol. Biol.* **17**, 1233–1240 (2010).
11. Shen, P. S. et al. Protein synthesis. Rqc2p and 60S ribosomal subunits mediate mRNA-independent elongation of nascent chains. *Science* **347**, 75–78 (2015).
12. Shao, S., Brown, A., Santhanam, B. & Hegde, R. S. Structure and assembly pathway of the ribosome quality control complex. *Mol. Cell* **57**, 433–444 (2015).
13. Shao, S. & Hegde, R. S. Reconstitution of a minimal ribosome-associated ubiquitination pathway with purified factors. *Mol. Cell* **55**, 880–890 (2014).
14. Lyumkis, D. et al. Structural basis for translational surveillance by the large ribosomal subunit-associated protein quality control complex. *Proc. Natl. Acad. Sci. USA* **111**, 15981–15986 (2014).
15. Shao, S., von der Malsburg, K. & Hegde, R. S. Listerin-dependent nascent protein ubiquitination relies on ribosome subunit dissociation. *Mol. Cell* **50**, 637–648 (2013).
16. Bengtson, M. H. & Joazeiro, C. A. Role of a ribosome-associated E3 ubiquitin ligase in protein quality control. *Nature* **467**, 470–473 (2010).
17. Osuna, B. A., Howard, C. J., Kc, S., Frost, A. & Weinberg, D. E. In vitro analysis of RQC activities provides insights into the mechanism and function of CAT tailing. *eLife* **6**, e27949 (2017).
18. Kostova, K. K. et al. CAT-tailing as a fail-safe mechanism for efficient degradation of stalled nascent polypeptides. *Science* **357**, 414–417 (2017).
19. Choe, Y. J. et al. Failure of RQC machinery causes protein aggregation and proteotoxic stress. *Nature* **531**, 191–195 (2016).
20. Defenouillere, Q., Zhang, E., Namane, A., Mouaikel, J., Jacquier, A. & Fromont-Racine, M. Rqc1 and Ltn1 prevent C-terminal alanine-threonine tail (CAT-tail)-induced protein aggregation by efficient recruitment of Cdc48 on stalled 60S subunits. *J. Biol. Chem.* **291**, 12245–12253 (2016).
21. Yonashiro, R. et al. The Rqc2/Tae2 subunit of the ribosome-associated quality control (RQC) complex marks ribosome-stalled nascent polypeptide chains for aggregation. *eLife* **5**, e11794 (2016).
22. Izawa, T., Park, S. H., Zhao, L., Hartl, F. U. & Neupert, W. Cytosolic protein Vms1 links ribosome quality control to mitochondrial and cellular homeostasis. *Cell* **171**, 890–903.e18 (2017).
23. Heo, J. M. et al. A stress-responsive system for mitochondrial protein degradation. *Mol. Cell* **40**, 465–480 (2010).
24. Heo, J. M., Nielson, J. R., Dephoure, N., Gygi, S. P. & Rutter, J. Intramolecular interactions control Vms1 translocation to damaged mitochondria. *Mol. Biol. Cell.* **24**, 1263–1273 (2013).
25. Jefferies, H. B., Reinhard, C., Kozma, S. C. & Thomas, G. Rapamycin selectively represses translation of the "polypyrimidine tract" mRNA family. *Proc. Natl. Acad. Sci. USA* **91**, 4441–4445 (1994).
26. Jefferies, H. B., Fumagalli, S., Dennis, P. B., Reinhard, C., Pearson, R. B. & Thomas, G. Rapamycin suppresses 5'TOP mRNA translation through inhibition of p70s6k. *EMBO J.* **16**, 3693–3704 (1997).
27. Shoemaker, C. J. & Green, R. Translation drives mRNA quality control. *Nat. Struct. Mol. Biol.* **19**, 594–601 (2012).
28. Yang J., Hao X., Cao X., Liu B. & Nystrom T. Spatial sequestration and detoxification of Huntingtin by the ribosome quality control complex. *eLife* **5**, e11792 (2016).
29. Meaux, S. & Van Hoof, A. Yeast transcripts cleaved by an internal ribozyme provide new insight into the role of the cap and poly(A) tail in translation and mRNA decay. *RNA* **12**, 1323–1337 (2006).
30. Yogev, O., Karniely, S. & Pines, O. Translation-coupled translocation of yeast fumarase into mitochondria in vivo. *J. Biol. Chem.* **282**, 29222–29229 (2007).
31. Nielson, J. R. et al. Sterol oxidation mediates stress-responsive Vms1 translocation to mitochondria. *Mol. Cell* **68**, 673–685 (2017). e676.
32. Holm, L. & Rosenstrom, P. Dali server: conservation mapping in 3D. *Nucleic Acids Res.* **38**, W545–W549 (2010).
33. Song, H. et al. The crystal structure of human eukaryotic release factor eRF1--mechanism of stop codon recognition and peptidyl-tRNA hydrolysis. *Cell* **100**, 311–321 (2000).
34. Graille, M., Chaillet, M. & van Tilbeurgh, H. Structure of yeast Dom34: a protein related to translation termination factor Erf1 and involved in No-Go decay. *J. Biol. Chem.* **283**, 7145–7154 (2008).
35. Brown, A., Shao, S., Murray, J., Hegde, R. S. & Ramakrishnan, V. Structural basis for stop codon recognition in eukaryotes. *Nature* **524**, 493–496 (2015).
36. Chu, J. et al. A mouse forward genetics screen identifies LISTERIN as an E3 ubiquitin ligase involved in neurodegeneration. *Proc. Natl. Acad. Sci. USA* **106**, 2097–2103 (2009).

Author contributions

O.Z.R., E.K.F., C.J.H., C.P.H., J.R, and A.F. designed the study and wrote the manuscript. N.D.T. and J.V.V. ran the polysome assays. O.Z.R., E.K.F., and C.J.H. collected the data. J.V.V. and S.F. generated plasmid constructs and yeast strains. C.P.H. helped with structural analyses. R.K. performed structural homology modeling and alignments. B.A.O. helped with the IVT assays. P.S.S. helped with the co-immunoprecipitation experiments. All authors commented and approved of the final manuscript.

Additional information

Supplementary Information accompanies this paper at https://doi.org/10.1038/s41467-018-04564-3.

Competing interests: The authors declare no competing interests.

Reprints and permission information is available online at http://npg.nature.com/reprintsandpermissions/

Publisher's note: Springer Nature remains neutral with regard to jurisdictional claims in published maps and institutional affiliations.